The Astrophysical Journal Letters, 835:L4 (5pp), 2017 January 20 doi:10.3847/2041-8213/835/1/L4

The Global and Small-scale Magnetic Fields of Fully Convective, Rapidly Spinning M Dwarf Pair GJ65 A and B

Oleg Kochukhov and Alexis Lavail
Department of Physics and Astronomy, Uppsala University, Box 516, Uppsala SE-75120, Sweden
Received 2016 November 23; revised 2016 December 12; accepted 2016 December 13; published 2017 January 16

Abstract

The nearby M dwarf binary GJ65 AB, also known as BL Cet and UV Cet, is a unique benchmark for investigation of dynamo-driven activity of low-mass stars. Magnetic activity of GJ65 was repeatedly assessed by indirect means, such as studies of flares, photometric variability, X-ray, and radio emission. Here, we present a direct analysis of large-scale and local surface magnetic fields in both components. Interpreting high-resolution circular polarization spectra (sensitive to a large-scale field geometry) we uncovered a remarkable difference of the global stellar field topologies. Despite nearly identical masses and rotation rates, the secondary exhibits an axisymmetric, dipolar-like global field with an average strength of 1.3 kG while the primary has a much weaker, more complex, and non-axisymmetric 0.3 kG field. On the other hand, an analysis of the differential Zeeman intensification (sensitive to the total magnetic flux) shows the two stars having similar magnetic fluxes of 5.2 and 6.7 kG for GJ65 A and B, respectively, although there is evidence that the field strength distribution in GJ65 B is shifted toward a higher field strength compared to GJ65 A. Based on these complementary magnetic field diagnostic results, we suggest that the dissimilar radio and X-ray variability of GJ65 A and B is linked to their different global magnetic field topologies. However, this difference appears to be restricted to the upper atmospheric layers but does not encompass the bulk of the stars and has no influence on the fundamental stellar properties.

Key words: stars: activity – stars: individual (GJ65 AB (BL Cet, UV Cet)) – stars: late-type – stars: magnetic field

1. Introduction

The red dwarf binary system GJ65 consists of two active flare M stars, BL Cet and UV Cet, in a wide orbit ($P_{\rm orb} = 26.3$ years). This binary is a prototype low-mass flare object, repeatedly targeted by photometric, radio, and X-ray observations (e.g., Schmitt et al. 2016). Studies that are able to resolve the GJ65 components indicate that both are M5.5–M6 (Henry et al. 1994), rapidly rotating, and spotted (Barnes et al. 2016) dwarfs with nearly identical masses and radii (Kervella et al. 2016), but a significantly different radio and X-ray behavior (Audard et al. 2003 and references therein).

Here, we take advantage of the recent refinement of the fundamental parameters of GJ65 by interferometry and high-contrast imaging (Kervella et al. 2016) and an accurate spectroscopic determination of the rotational properties of the components (Barnes et al. 2016) to characterize magnetic field strength and topology in both stars. These direct constraints on the surface stellar magnetic field are essential for understanding dynamo action in fully convective stars and interpreting activity patterns of the GJ65 components.

2. Observational Data

High spectral resolution circular polarization observations of GJ65 A and B were obtained with the ESPaDOnS spectropolarimeter attached to the Canada–France–Hawaii Telescope (CFHT). The binary system was observed on the night of 2013 September 21, when four spectra of GJ65 A and four spectra of GJ65 B were recorded, and on the night of 2013 September 24, when another four spectra of GJ65 B were obtained. According to the orbital parameters derived by Kervella et al. (2016), the projected separation of the components was $2\farcs2$ at the time of ESPaDOnS observations, implying that the stars were well isolated by the $1\farcs6$ instrument aperture.

Each spectropolarimetric observation of GJ65 AB consisted of four 480 s sub-exposures obtained with different polarimeter configurations. The resulting Stokes I and V spectra, retrieved from the CFHT Science Archive[1], were reduced by the UPENA pipeline using the LIBRE-ESPRIT software (Donati et al. 1997). These spectra cover the 370–1050 nm wavelength interval at a resolution of about $R = 65{,}000$ and have a peak signal-to-noise ratio (S/N) of 200–300 per pixel.

The information about individual observations of GJ65 AB are provided in Table 1, which lists the mid-exposure times, S/Ns, and rotation phases calculated with the period of $P = 0.2432$ day for GJ65 A and $P = 0.2269$ day for GJ65 B (Barnes et al. 2016).

3. Magnetic Field Analysis

3.1. Global Magnetic Field Topology

The quality of ESPaDOnS polarization observations of GJ65 is insufficient for an analysis of polarization signatures in individual spectral lines. Consequently, we applied the least-squares deconvolution procedure (LSD; Donati et al. 1997; Kochukhov et al. 2010) to derive high S/N mean Stokes V profiles based on a line mask containing 1690 atomic absorption lines deeper than 0.2 of the continuum. The LSD atomic line mask was derived from a line list retrieved from the VALD3 database (Ryabchikova et al. 2015) using $T_{\rm eff} = 2900$ K, $\log g = 5.0$ MARCS model atmosphere (Gustafsson et al. 2008). Application of LSD yielded an S/N gain of about 20, allowing us to detect circular polarization signals in all observations of both components.

Examination of the LSD Stokes V profiles of GJ65 A and B reveals a stark difference between the two stars. As

[1] http://www.cadc-ccda.hia-iha.nrc-cnrc.gc.ca/en/cfht/

Table 1
Journal of Spectropolarimetric Observations of GJ65 AB

HJD	Phase	S/N	$\langle B_z \rangle$ (G)
GJ65 A (BL Cet)			
2456556.9601	0.111	314	146 ± 19
2456556.9854	0.214	294	167 ± 20
2456557.0628	0.533	281	41 ± 23
2456557.0883	0.638	282	37 ± 20
GJ65 B (UV Cet)			
2456556.9332	0.000	260	449 ± 21
2456557.0114	0.344	237	555 ± 21
2456557.0368	0.456	239	392 ± 22
2456557.1184	0.816	246	543 ± 21
2456559.9364	0.236	244	660 ± 22
2456559.9943	0.491	253	386 ± 19
2456560.0521	0.745	244	673 ± 21
2456560.1062	0.984	203	412 ± 25

Note. The rotational phase reported in the second column is computed using the periods from Barnes et al. (2016) and the reference Julian date of the first observation of GJ65 B.

demonstrated by Figure 1, the primary shows low-amplitude polarization signatures that change significantly from one observation to the next. On the other hand, the secondary consistently exhibits morphologically simpler and stronger antisymmetric signatures indicative of a positive large-scale magnetic field. The mean longitudinal magnetic field $\langle B_z \rangle$, estimated from the first moment of the Stokes V LSD profiles (Wade et al. 2000) and reported in the last column of Table 1, ranges from +400 to +700 G for GJ65 B and from 0 to +150 G for GJ65 A.

We further analyzed the Stokes V LSD profiles of GJ65 with the Zeeman Doppler imaging (ZDI; Kochukhov 2016) inversion technique to obtain detailed field topology models. ZDI was previously applied to a sample of active M dwarf stars of different masses by Donati et al. (2008), Morin et al. (2008, 2010), and Hébrard et al. (2016). These studies revealed global fields with strengths up to several kG and demonstrated that early-M, partially convective dwarfs typically have weak and complex magnetic field structures, while mid-M stars tend to show strong axisymmetric dipolar field topologies, and late-M, fully convective dwarfs exhibit a mixture of both types of field geometries (see the review by Morin 2012).

Our ZDI analysis of GJ65 was carried out with the code described by Kochukhov et al. (2014) and Rosén et al. (2016). Similar to the latter paper, the local Stokes parameter profiles were approximated with the Unno–Rachkovsky solution of the polarized radiative transfer equations (Landi Degl'Innocenti & Landolfi 2004). The central wavelength and effective Landé factor of the model profiles were adopted according to the average values of the LSD line mask; the line strength was adjusted to match the equivalent width of the observed LSD intensity profile.

The magnetic field was represented using a spherical harmonic expansion, with the maximum angular degree $\ell_{\max} = 5$. The magnetic inversions were regularized by penalizing a contribution of higher ℓ modes (see Kochukhov et al. 2014). This magnetic mapping methodology is very similar to previous applications of ZDI to active mid- and late-M dwarfs (Morin et al. 2008, 2010) with the exception that here we do not apply global field filing factors to improve the fit to the observed Stokes V profiles. Furthermore, since observations of GJ65 cover about 10%–14% of the rotation cycles of the components, we accounted for the phase smearing by integrating the model LSD profiles over appropriate phase intervals.

The eight spectropolarimetric observations of GJ65 B have an adequate phase coverage to obtain a detailed map of the surface magnetic field. On the other hand, the four spectra available for GJ65 A cover only about half of the rotational period. Nevertheless, this data set is sufficient to derive an approximate ZDI map that can be meaningfully compared with the inversion results for GJ65 B.

Taking into account results of the Stokes I DI modeling by Barnes et al. (2016), we adopted projected rotational velocities $v \sin i = 28.6$ km s^{-1} for GJ65 A and 32.0 km s^{-1} for GJ65 B, respectively, and an inclination angle of $i = 60°$ for both stars. This value agrees within error bars with the inclination angles that follow from the above $v \sin i$, the rotation periods determined by Barnes et al. (2016), and the radii measured by Kervella et al. (2016).

The global magnetic field maps of GJ65 AB are presented in Figure 1 along with a comparison of the observed and computed LSD Stokes V profiles. It is evident that the large-scale field of GJ65 B (peak local strength 2.34 kG, mean strength 1.34 kG) is considerably stronger than the field of GJ65 A (peak local strength 0.84 kG, mean strength 0.34 kG). The field of GJ65 B is also predominantly dipolar (92% of the field energy is contained in $\ell = 1$ components) and axisymmetric (89% of the energy is in $m < \ell/2$ components). In contrast, the field of GJ65 A has a larger contribution of higher-ℓ(70% of the energy is in $\ell = 1$ components) and non-axisymmetric (56% of the energy is in $m < \ell/2$ components) modes. The fields of both stars are largely poloidal (89%–93% of the energy is in poloidal components).

Details of the field topology of GJ65 A are less precisely determined than for the B component due to an incomplete phase coverage obtained for the primary. Nevertheless, the basic conclusion that the primary's field structure must be less axisymmetric and more complex is supported by the complex Stokes V LSD line shapes observed at phases 0.533 and 0.638. Such Stokes V profile morphologies are not observed in any of the eight observations available for GJ65 B.

3.2. Total Magnetic Flux

An analysis of Zeeman broadening and intensification of spectral lines enables an estimate of the total magnetic flux, which contains contributions of both the large-scale field and the small-scale magnetic structures unresolved by polarimetry. Previous studies applied this diagnostic method to atomic and molecular lines in the Stokes I spectra of many low-mass stars and brown dwarfs, detecting fields with typical strengths of 2–4 kG (Johns-Krull & Valenti 1996; Reiners & Basri 2007; Reiners et al. 2009; Shulyak et al. 2014). In a recent study by D. Shulyak (2017, in preparation; see also summary in Kochukhov et al. 2017) magnetic fields of up to 6.4 kG were found in several active, rapidly rotating ($P_{\rm rot} = 0.4$–0.8 days) M4–6 dwarfs. The GJ65 components are spinning about a factor of two faster than any of the M dwarf stars with direct magnetic field measurements in the literature.

Our field strength measurements take advantage of a group of Ti I lines at λ 9744–9788 Å. These lines correspond to the

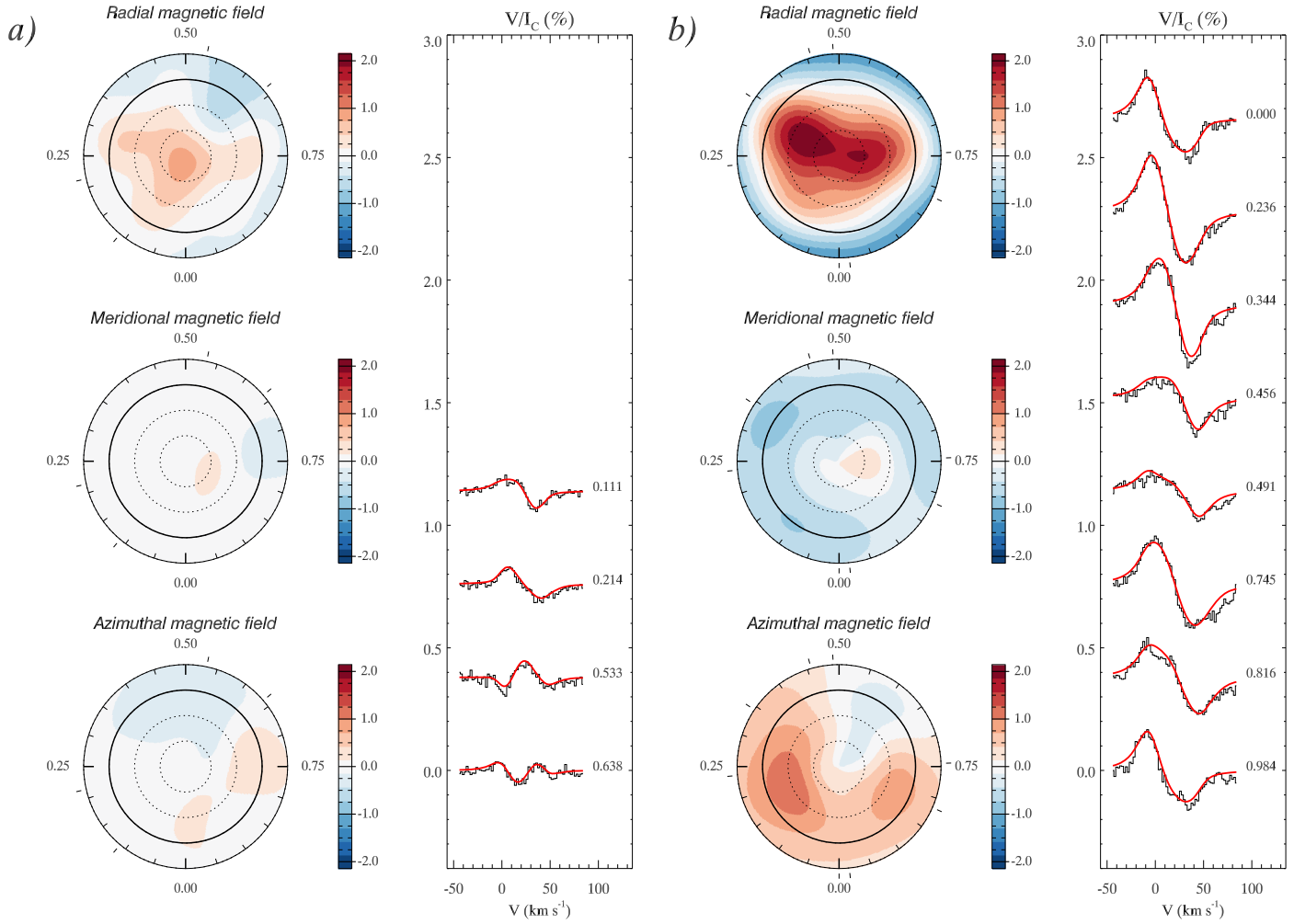

Figure 1. Global magnetic field geometry derived for GJ65 A (a) and GJ65 B (b) with Zeeman Doppler imaging. For each star the flattened polar projections of the radial, meridional, and azimuthal magnetic field components are presented on the left. The color bars indicate the field strength in kG. A comparison between the observed (histograms) and model (solid lines) Stokes *V* profiles are shown on the right. The spectra for different rotational phases are offset vertically.

transitions between similar energy levels, hence the relative scale of their oscillator strengths, obtained from VALD, is well-known. One of these lines, Ti I 9743.61 Å has zero effective Landé factor, meaning that this spectral feature is entirely insensitive to magnetic field. Then, a magnetic field strength can be determined using a differential spectrum synthesis analysis of magnetically sensitive lines, e.g., Ti I 9770.30, 9783.31, 9787.69 Å, relative to Ti I 9743.61 Å. This magnetic intensification diagnostic does not rely on interpreting details of the line profile shapes and therefore can be applied to rapidly rotating stars, such as the GJ65 components.

Some of the Ti I lines mentioned above are significantly affected by the telluric absorption features. We used the MOLECFIT tool (Smette et al. 2015) to model the telluric spectrum and remove its contribution from stellar observations. Then, the four spectra of GJ65 A and eight spectra of GJ65 B were averaged, yielding high-quality intensity spectra for each star.

The magnetic field effects on the Ti I lines were studied with the help of the SYNMAST code (Kochukhov et al. 2010), which solves the polarized radiative transfer equation at several limb angles for a given line list, model atmosphere, and prescribed magnetic field strength and orientation. In this study, we adopted a homogeneous radial magnetic field. This assumption has no bearing on the final analysis results since the disk-integrated Stokes *I* spectra are not particularly sensitive to the field orientation and, in any case, sample a wide range of field orientations with respect to the observer for any field geometry.

Based on the radii and masses given by Kervella et al. (2016), we adopted $\log g = 5.1$ for both components of GJ65 and used the solar-metallicity MARCS model atmospheres with $T_{\rm eff} = 3000$ K for the primary and 2900 K for the secondary. The probable effective temperature uncertainty of $\sim$100 K does not introduce significant differential effects for the studied Ti I lines.

For both GJ65 A and B our spectrum synthesis reproduces the observed width and intensity of Ti I 9743.61 Å with the solar abundance of titanium and $v \sin i$ given by Barnes et al. (2016). At the same time, the three other Ti I lines are clearly too weak without a magnetic field (see Figure 2). Adjusting the field strength to match the observed intensity of each of these lines separately, we found $\langle B \rangle = 5.0 \pm 0.5$ kG for GJ65 A and $\langle B \rangle = 5.7 \pm 0.6$ kG for GJ65 B, with the error bars corresponding to the scatter of measurements derived from individual lines.

As illustrated by Figure 2, theoretical spectrum for a 5 kG field covering the entire stellar surface provides a satisfactory fit to all Ti I lines in GJ65 A. However, magnetically sensitive

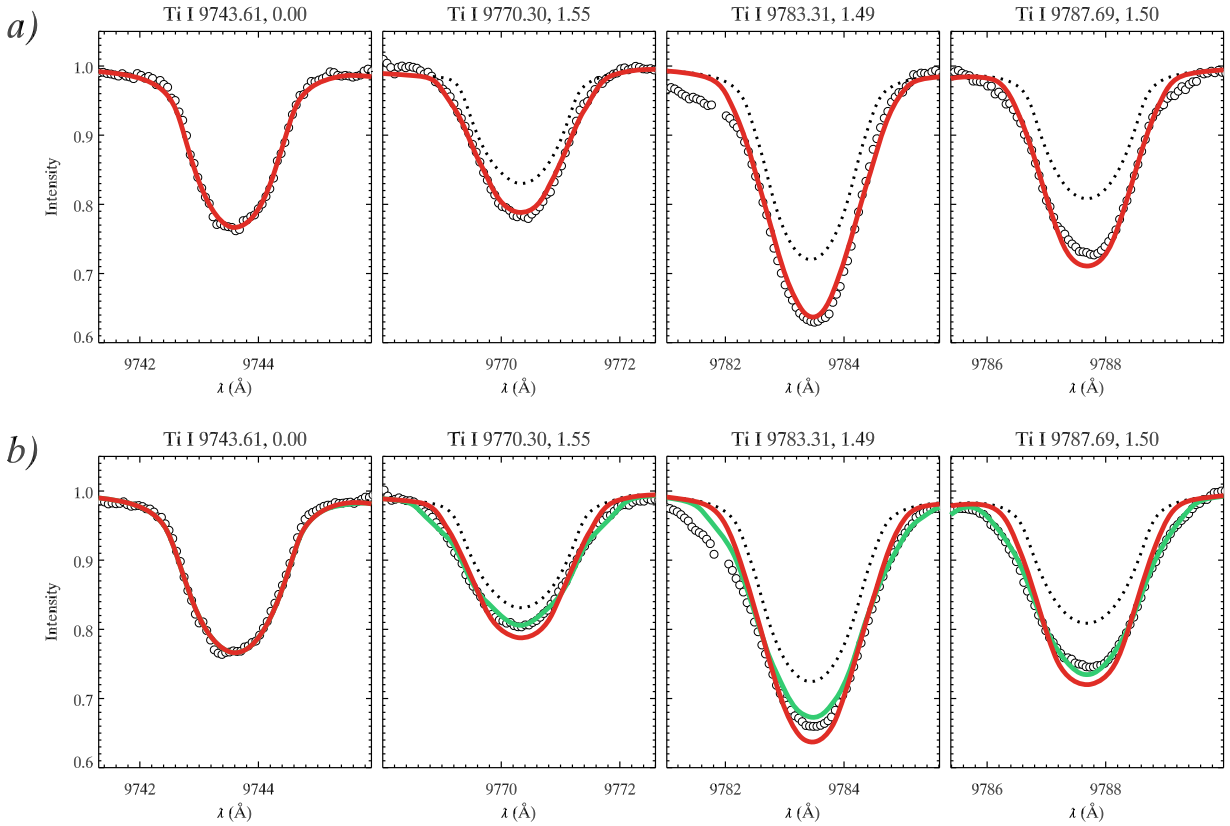

Figure 2. Magnetic intensification and broadening analysis for GJ65 A (a) and GJ65 B (b) using the four Ti I spectral lines at λ 9743.6–9787.7 Å. The average observed spectra (open circles) are compared with a non-magnetic synthetic spectrum (dotted line) and with calculations for a 5 kG field covering the entire stellar surface (red line). In addition, the green line in panel (b) illustrates calculations for a 10 kG field covering 60% of the stellar surface. The central wavelengths of the transitions and their effective Landé factors are indicated above each panel.

lines in GJ65 B exhibit a more triangular shape than predicted by calculations. This anomaly is not observed for the Ti I 9743.61 Å line in GJ65 B and is not seen for any of the Ti I lines in GJ65 A. This suggests the presence of a strong-field component in the field distribution in GJ65 B, which is responsible for the extended wings of magnetically sensitive lines. To test this hypothesis, we applied to both stars a two-component model fit, combining a non-magnetic spectrum with calculations for a given field strength covering a fraction f of the stellar surface. This model succeeds in improving the fit to GJ65 B spectra (see Figure 2), yielding $B = 10.5 \pm 1.2$ kG, $f = 0.6 \pm 0.1$, and $\langle B \rangle = B\ f = 6.7 \pm 0.6$ kG. On the other hand, results of the two-component model fit for GJ65 A ($B = 6.0 \pm 1.5$ kG, $f = 0.9 \pm 0.1$, and $\langle B \rangle = Bf = 5.2 \pm 0.5$ kG) are compatible with the single-component fit.

These results were obtained using the mean spectra of GJ65 AB. We have also examined individual observations, finding no appreciable variability of the Ti I lines in GJ65 A. The secondary component, on the other hand, shows a weak rotational modulation of Ti I line shapes. This variability, illustrated in Figure 3, appears to be magnetic in nature because it is absent in the magnetic null line Ti I 9743.61 Å but present in other Ti I transitions. Fitting the phase resolved spectra of GJ65 B with the two-component model described above reveals a coherent, single-wave variation of B from 8 to 11 kG and $\langle B \rangle$ from 5.7 to 7.0 kG, with the maximum of both parameters occurring at phase 0.5. To our knowledge, this is the first report of a rotational modulation of the magnetic field intensity derived from Stokes I spectra of an M dwarf.

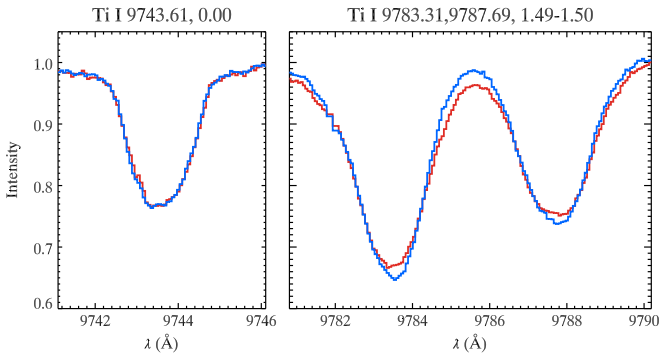

Figure 3. Illustration of the variability of Ti I lines in GJ65 B. The average over three observations in the 0.34–0.49 phase interval (red curve) is compared with the mean of another three spectra in the 0.82–1.00 phase interval (blue curve). The left panel shows the magnetic null line Ti I 9743.61 Å. The right panel shows two Ti I lines with Landé factors 1.49–1.50.

4. Discussion

In this Letter, we analyzed the global magnetic field topology and measured the total magnetic flux for both components of the well-known active M dwarf binary GJ65. The components of this system, BL Cet and UV Cet, are the fastest spinning fully convective stars for which direct magnetic field measurements are now available. Despite similarity of their fundamental parameters and spin rates, these stars exhibit drastically different global magnetic fields. The secondary, UV Cet, has a strong, axisymmetric dipolar field. The primary, BL Cet, has a more complex global field structure, with the

magnetic energy more than an order of magnitude weaker than for UV Cet. This difference in the global field organization may be responsible for a significantly different radio and X-ray variability of the two stars, with UV Ceti being both more luminous and variable (Audard et al. 2003). Our results thus suggest that the radio and X-ray behavior of GJ65 B is linked to an extended magnetosphere anchored in its strong global field, which GJ65 A lacks.

The puzzling finding of very different global fields in nearly identical objects demonstrates that the dynamo in fully convective stars is not a straightforward function of fundamental stellar parameters. The coexistence of different types of large-scale fields in similar late-M dwarfs was previously found by Morin et al. (2010) based on a heterogeneous sample of objects with uncertain relative ages and evolutionary histories. Our finding of the discrepant global fields in well-characterized, coeval components of GJ65 strengthens these results and lends support to the hypothesis of convective dynamo bistability (Gastine et al. 2013).

An alternative interpretation of the coexistence of different types of field topologies in M dwarfs with similar fundamental parameters was suggested by Kitchatinov et al. (2014). These authors argued that M dwarfs have magnetic cycles and observations of qualitatively different field geometries correspond to different phases of these cycles. However, the consistently discrepant radio behavior of the GJ65 components, which appears to be linked to their different global field configurations, has been observed since the first high angular resolution radio studies of GJ65 (Gary & Linsky 1981). This implies that any cyclic evolution of the global field in GJ65 AB must occur on a timescale longer than $\sim$30 years.

At the same time, complementary analysis of the total magnetic flux reveals a different perspective on stellar magnetic fields. Similar to previous studies (e.g., Reiners & Basri 2009), we find that up to 95% of the field energy is contained in small-scale field. Moreover, the total mean field strengths derived for GJ65 A and B (5.2 and 6.7 kG, respectively) are similar, although there is an evidence of different field strength distributions, with the field in GJ65 B featuring rotationally modulated, strong-field component absent in GJ65 A. These results, inferred from the analysis of Zeeman intensification, indicate that the discrepant global field topologies diagnosed by polarimetry are limited to superficial stellar layers and immediate circumstellar environment but do not encompass the bulk of the stars. This picture contradicts theoretical bistable dynamo models that predict a different total field strength and different internal field for the two dynamo branches (Gastine et al. 2012, 2013).

On the other hand, Kervella et al. (2016) reported the same 12%–14% discrepancy between the observed and theoretically computed radii of the GJ65 components. Since the interior magnetic field is the most likely culprit for the inflated radii of active low-mass stars (Chabrier et al. 2007; Feiden & Chaboyer 2012), GJ65 A and B should have comparable interior fields, which is in line with our finding of the similar total surface magnetic fluxes.

The authors acknowledge support by the Knut and Alice Wallenberg Foundation, the Swedish Research Council, and the Swedish National Space Board.

This Letter is based on archival spectropolarimetric observations obtained at the CFHT, which is operated by the National Research Council of Canada, the Institut National des Sciences de l'Univers (INSU) of the Centre National de la Recherche Scientifique (CNRS) of France, and the University of Hawaii.

References

Audard, M., Güdel, M., & Skinner, S. L. 2003, ApJ, 589, 983
Barnes, J., Haswell, C., Jeffers, S., et al. 2016, in The 19th Cambridge Workshop on Cool Stars, Stellar Systems, and The Sun, ed. G. Feiden (Uppsala: Zenodo), 132
Chabrier, G., Gallardo, J., & Baraffe, I. 2007, A&A, 472, L17
Donati, J.-F., Morin, J., Petit, P., et al. 2008, MNRAS, 390, 545
Donati, J.-F., Semel, M., Carter, B. D., Rees, D. E., & Collier Cameron, A. 1997, MNRAS, 291, 658
Feiden, G. A., & Chaboyer, B. 2012, ApJ, 757, 42
Gary, D. E., & Linsky, J. L. 1981, ApJ, 250, 284
Gastine, T., Duarte, L., & Wicht, J. 2012, A&A, 546, A19
Gastine, T., Morin, J., Duarte, L., et al. 2013, A&A, 549, L5
Gustafsson, B., Edvardsson, B., Eriksson, K., et al. 2008, A&A, 486, 951
Henry, T. J., Kirkpatrick, J. D., & Simons, D. A. 1994, AJ, 108, 1437
Hébrard, É. M., Donati, J.-F., Delfosse, X., et al. 2016, MNRAS, 461, 1465
Johns-Krull, C. M., & Valenti, J. A. 1996, ApJL, 459, L95
Kervella, P., Mérand, A., Ledoux, C., Demory, B.-O., & Le Bouquin, J.-B. 2016, A&A, 593, A127
Kitchatinov, L. L., Moss, D., & Sokoloff, D. 2014, MNRAS, 442, L1
Kochukhov, O. 2016, in Lecture Notes in Physics, Vol. 914, ed. J.-P. Rozelot & C. Neiner (Basel: Springer International), 177
Kochukhov, O., Lüftinger, T., Neiner, C., Alecian, E. & MiMeS Collaboration 2014, A&A, 565, A83
Kochukhov, O., Makaganiuk, V., & Piskunov, N. 2010, A&A, 524, A5
Kochukhov, O., Petit, P., Strassmeier, K. G., et al. 2017, AN, in press (arXiv:1612.03388)
Landi Degl'Innocenti, E., & Landolfi, M. 2004, Polarization in Spectral Lines, Vol. 307 (Dordrecht: Kluwer)
Morin, J. 2012, in EAS Publ. Ser., Vol. 57, ed. C. Reylé, C. Charbonnel, & M. Schultheis (Les Ulis: EDP Sciences), 165
Morin, J., Donati, J.-F., Petit, P., et al. 2008, MNRAS, 390, 567
Morin, J., Donati, J.-F., Petit, P., et al. 2010, MNRAS, 407, 2269
Reiners, A., & Basri, G. 2007, ApJ, 656, 1121
Reiners, A., & Basri, G. 2009, A&A, 496, 787
Reiners, A., Basri, G., & Browning, M. 2009, ApJ, 692, 538
Rosén, L., Kochukhov, O., Hackman, T., & Lehtinen, J. 2016, A&A, 593, A35
Ryabchikova, T., Piskunov, N., Kurucz, R. L., et al. 2015, PhyS, 90, 054005
Schmitt, J. H. M. M., Kanbach, G., Rau, A., & Steinle, H. 2016, A&A, 589, A48
Shulyak, D., Reiners, A., Seemann, U., Kochukhov, O., & Piskunov, N. 2014, A&A, 563, A35
Smette, A., Sana, H., Noll, S., et al. 2015, A&A, 576, A77
Wade, G. A., Donati, J.-F., Landstreet, J. D., & Shorlin, S. L. S. 2000, MNRAS, 313, 851